Ultrathin initiated chemical vapor deposition polymer interfacial energy control for directed self-assembly hole-shrink applications

Moshe Dolejsi, Priya Moni, Cody T. Bezik, Chun Zhou, Juan J. de Pablo, Karen K. Gleason, and Paul F. Nealey

Citation: Journal of Vacuum Science & Technology B **37**, 061804 (2019); doi: 10.1116/1.5121541
View online: https://doi.org/10.1116/1.5121541
View Table of Contents: https://avs.scitation.org/toc/jvb/37/6
Published by the American Vacuum Society

Ultrathin initiated chemical vapor deposition polymer interfacial energy control for directed self-assembly hole-shrink applications

Moshe Dolejsi,[1] Priya Moni,[2] Cody T. Bezik,[1] Chun Zhou,[1] Juan J. de Pablo,[1] Karen K. Gleason,[2] and Paul F. Nealey[1,a)]
[1]*Pritzker School of Molecular Engineering, University of Chicago, Chicago, Illinois 60637*
[2]*Department of Chemical Engineering, Massachusetts Institute of Technology, Cambridge, Massachusetts 02139*

(Received 25 July 2019; accepted 11 September 2019; published 7 October 2019)

Integrated circuit layouts consist of patterned lines and holes, where holes define the electrical contacts between adjacent layers. Block copolymer directed self-assembly (DSA) successfully shrinks the critical dimension (CD) of these contacts beyond the resolution of conventional lithography. DSA also radically improves the CD uniformity. One particularly difficult step of the DSA hole-shrink process involves establishing the correct interfacial energy throughout a lithographically templated hole to ensure good assembly. Initiated chemical vapor deposition (iCVD) is a uniform, ultrathin, ultraconformal, all-organic deposition technique that allows for precise control of the interfacial energy. In this work, the authors use iCVD of polydivinylbenzene at film thicknesses below 5 nm to blend the interfacial energy of the coated film with that of the silicon/spin-on carbon template. They fully characterize the iCVD surface by means of two liquid surface energy measurements. They further identify the interfacial energies presented by these functionalized templates through qualitative hole-island tests as well as quantitative harmonic mean estimations. In parallel, the authors run theoretically informed coarse grained simulations with the determined interaction parameters and DSA experiments and find good agreement across the range of chemistries created. Through careful control of iCVD conditions, especially filament temperature, they achieve a strong polystyrene-preferential sidewall with a nonpreferential bottom which they then demonstrate, both in the simulation and in the experiment, allows for a successful hole-shrink process across a wide range of template hole diameters. *Published by the AVS.* https://doi.org/10.1116/1.5121541

I. INTRODUCTION

High volume manufacturing of smaller and smaller features requires increasing control over size, shape, and uniformity. Bottom-up processes such as directed self-assembly (DSA) are uniquely posed to address all three requirements. In DSA, a lithographically defined template anchors and guides the self-assembly of block copolymers (BCP) to form sublithographic features with excellent uniformity.[1–6] The patterning of contact holes or via holes is of particular interest, as multiple complex 193i exposures are required to achieve the proper density.[7–9] Even with extreme ultraviolet (EUV) lithography, which provides the ability to pattern at higher densities, DSA hole-shrink has been shown to improve EUV local critical dimension uniformity and repair stochastic defects such as merging vias.[10] In the DSA contact hole-shrink process, a lithographically defined template is often etched into spin-on carbon (SOC) using a spin-on glass (SOG) and SOC transfer stack.[8,9,11,12] This template consists of an SOC sidewall with a silicon or silicon nitride bottom. Subsequent functionalization provides the appropriate chemical cue to the BCP to assemble into structures perpendicular to the surface.

In order to achieve the highest resolution features with the highest density, polystyrene-*block*-poly(methyl methacrylate) (PS-*b*-PMMA), with the appropriate size and volume fraction to form PMMA minority cylinders, is assembled inside the functionalized template. Etching removes the PMMA cylinders and transfers their pattern into the underlying dielectric material, which is subsequently metallized to create a contact or via. Particularly advantageous to reaching high density is the ability to assemble multiple such contacts with a single lithographic template.[8,9,13] Numerous simulations of self-assembly in confinement highlight the importance of independently functionalizing the side and bottom of the template to ensure a through-film structure.[13–16] As a result, numerous experimental efforts have focused on achieving different functionalities on the sidewall versus the bottom of the template. Gronheid *et al.* pioneered the sequential use of two orthogonal brush chemistries for this purpose.[9] A related approach, developed by Zhou *et al.,* uses kinetic control to achieve differing brush thickness on the sidewall and template bottom, allowing for either the interfacial energy of the brush or a mixture of the brush and substrate to be presented.[11] These efforts, as well as new simulations, have revealed unexpectedly that the strength of the sidewall preference is the key to avoid defective structures during the hole-shrink process.[11,16]

It is thus desirable to have a more controllable process for setting the interfacial energy throughout the template. Initiated chemical vapor deposition (iCVD) is an ultrathin, ultraconformal,[17] all-organic vapor phase deposition technique that allows for precise control of interfacial energy and has previously been integrated with DSA flows for lines and

Note: This paper is part of the Conference Collection: The 63rd International Conference on Electron, Ion, and Photon Beam Technology and Nanofabrication (EIPBN 2019).
a)Electronic mail: nealey@uchicago.edu

spaces.[18–21] In iCVD, a resistively heated filament cleaves a thermally labile bond in an initiator molecule. The resulting free radicals react with monomers adsorbed on a cooled growth surface to create a polymer film. The types of radicals generated and their relative concentration allow fine control of interfacial energy of the resulting polymer thin film. The radical mixture present in the chamber is largely dependent on the filament temperature.[22] In this work, we deposit at varying filament temperatures iCVD films that are thin enough (~5 nm) to present a mixed substrate/film interfacial energy. These interfacial energies are qualitatively determined through the hole-island test[23–25] and quantitatively determined through the harmonic mean approximation from surface energies.[26] The functionalized templates are then simulated to model the DSA process. Finally, DSA is performed and found to be in good agreement with simulations. As a result, we identify a processing window where iCVD can be used to perfectly functionalize a template and DSA can be successfully achieved.

II. EXPERIMENT

In this section, we describe the DSA hole-shrink process as outlined in Fig. 1, as well as the ancillary experiments and simulations performed to fully describe the process.

A. Materials

Highly doped silicon wafers, with resistance (R) < 0.1 Ω cm, were obtained from Pure Wafer or Silicon Materials, Inc. and cleaned with hot piranha immediately prior to use (DANGER! Reacts explosively with organics). SOC and SOG were provided by Tokyo Ohka Kogyo Co. (TOK) and used as received. Cylinder-forming PS-*b*-PMMA with a molecular weight of 50k-*b*-20k with a bulk morphological period (L_0) of 38 nm and lamellae-forming PS-*b*-PMMA with a molecular weight of 22k-*b*-22k with $L_0 = 25$ nm were purchased from Polymer Source and used as received. Positive e-beam resist CSAR 6200.04 was purchased from Allresist and diluted in propylene glycol monomethyl ether acetate to 2.5 wt. %. DVB (80%), di-*tert*-butyl peroxide (TBPO, 98%), isopropyl alcohol (IPA), deionized water (HPLC grade), and diiodomethane (99%) were purchased from Millipore Sigma and used without further purification. Oxygen (99%) and argon (99%) gases were purchased from Airgas and used without further purification.

B. Formation of hole-shrink templates

Lithographic templates were prepared following a process flow similar to that implemented by imec.[8] First SOC and then SOG were spin-coated and baked on a wafer in accordance with the manufacturer's instructions to yield a 100 nm thick layer of SOC and a 32 nm thick layer of SOG. A downstream oxygen clean was then used to oxidize the SOG surface to improve the e-beam resist adhesion. Diluted CSAR 6200 was spin-coated to a thickness of ~55 nm and soft baked at 150 °C. The resist was then exposed on a Raith EBPG 5000+ electron beam lithography tool using a single shot exposure for each hole with an effective dose of 400–800 μ C/cm^2. Development was performed in n-amyl acetate for 1 min followed by an IPA rinse and a nitrogen dry. A Plasmatherm ICP-RIE dedicated to fluorine chemistry was used to etch first the SOG with CF_4 and then the SOC with O_2 using a high bias power at low pressures. Finally, any remaining SOG was stripped in buffered HF before being shipped to MIT for iCVD deposition.

C. iCVD depositions conducted at MIT

Custom hole-shrink samples, clean silicon wafer sample, and SOC wafer samples were cleaned with an oxygen plasma (Harrick Plasma, RF Power 10.2 W, O_2 pressure 515–530 mTorr, 8 s exposure) prior to depositions. The samples were immediately loaded in a custom-built iCVD chamber, described elsewhere,[27] and brought under vacuum.

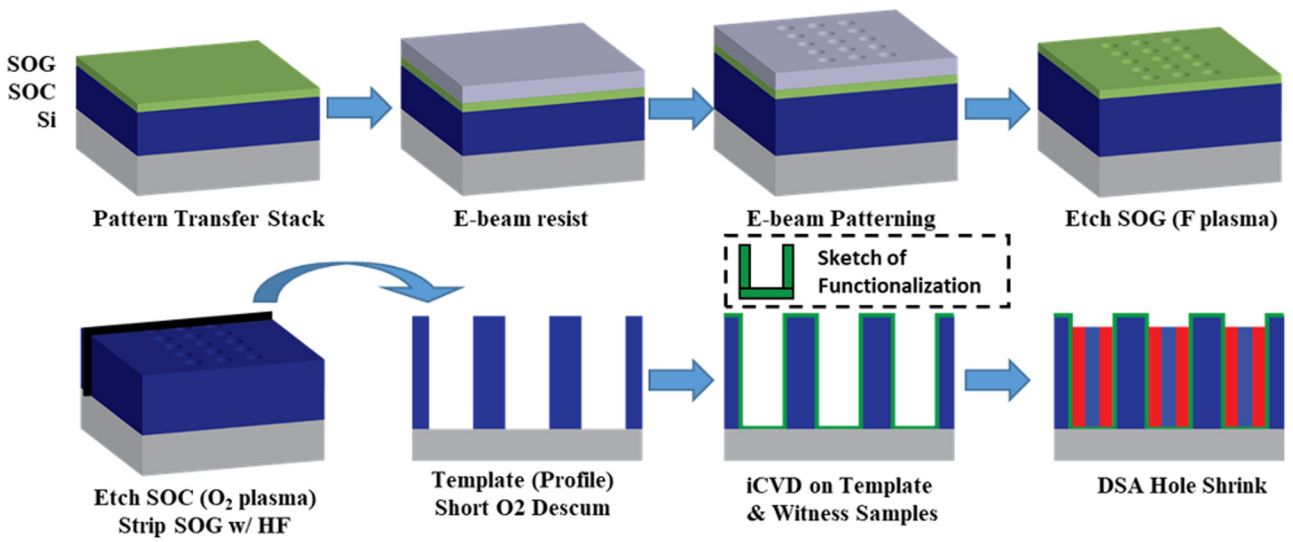

FIG. 1. Schematic showing the complete DSA hole-shrink process. The inset is a sketch that will be used to depict template preferentiality throughout the paper.

DVB was heated to 40 °C and the resulting vapors were metered into the chamber at 0.5 sccm using a heated mass flow controller (MKS instruments). Room temperature TBPO and argon were metered into the chamber at 3 and 6.7 sccm, respectively, using mass flow controllers. The chamber pressure was maintained at 90 mTorr using a throttling butterfly valve (MKS Instruments), and the substrate temperature was fixed at 30 °C using a recirculating chiller (Thermo Scientific). A Chromaloy O filament (Goodfellow) was resistively heated to crack the peroxide bond of TBPO molecules.

Three filament temperatures (240, 270, and 300 °C) and two film thicknesses per filament temperature were used, resulting in six experimental conditions. Previously, these filament temperatures were shown to yield slightly PS-preferential to very PS-preferential films.[19] The deposition time was varied to yield different film thicknesses. Films grown at higher filament temperatures required shorter deposition times. Film thickness on a reference silicon wafer (Pure Wafer) was measured *ex situ* using a variable angle spectroscopic ellipsometer (J. A. Woollam) at incident angles of 65°, 70°, and 75°. The data were fit to a Cauchy-Urbach isotropic model to extract the film thickness. A summary of the experimental conditions and the resulting polydivinylbenzene (PDVB) film thicknesses are given in Table I. Atomic force microscopy (AFM) of the templates both before and after deposition was measured using an ultrasharp, high frequency USC-F1.2-k7.3 tip on an Asylum Cypher in order to determine conformality.

D. Hole-island qualitative determination of interfacial energy

Symmetric PS-*b*-PMMA (22k-*b*-22k) was spin-coated to a thickness of $1.0L_0$, $1.25L_0$, and $1.5L_0$ onto both PDVB-coated silicon and SOC corresponding to each iCVD condition. Films were then annealed for 1 h in a vacuum chamber at 170 °C to induce microphase separation. Finally, films were imaged both optically and using a Zeiss Merlin SEM at a working distance of 3 mm, with an acceleration voltage of 1 keV in the high-resolution mode with the InLens secondary electron detector.

E. Quantitative determination of interfacial energy

Static contact angles of water and diiodomethane on the PDVB films grown on both silicon and SOC were measured using a Model 500 Ramé-Hart Goniometer. The dispersive (γ^d), polar (γ^p), and total surface energies (γ) were calculated assuming a harmonic mean using the DROP Advanced software included with the goniometer. Interfacial energies ($\gamma_{\text{interfacial}}$) between the substrates and either PS or PMMA were estimated using the harmonic mean equation, Eq. (1), as described previously.[26] The surface energies of PS and PMMA, Eqs. (2) and (3), were taken from the literature,[28]

$$\gamma_{\text{interfacial}} = \gamma_{\text{poly}} + \gamma_{\text{surf}} - \frac{4\gamma^d_{\text{poly}}\gamma^d_{\text{surf}}}{\gamma^d_{\text{poly}} + \gamma^d_{\text{surf}}} - \frac{4\gamma^p_{\text{poly}}\gamma^p_{\text{surf}}}{\gamma^p_{\text{poly}} + \gamma^p_{\text{surf}}}, \quad (1)$$

where

$$\gamma_{\text{PS}} = \gamma^d_{\text{PS}} + \gamma^p_{\text{PS}} = 33.9 + 6.8 = 40.7 \left(\frac{\text{mJ}}{\text{m}^2}\right) \quad (2)$$

and

$$\gamma_{\text{PMMA}} = \gamma^d_{\text{PMMA}} + \gamma^p_{\text{PMMA}} = 29.6 + 11.5 = 41.1 \left(\frac{\text{mJ}}{\text{m}^2}\right). \quad (3)$$

TABLE I. Experimental conditions and resulting PDVB film thickness.

Filament temperature (°C)	Deposition time (min)	Film thickness (nm)
240	60	4.1 ± 0.5
	30	3.4 ± 0.0
270	30	5.1 ± 0.9
	15	3.6 ± 0.3
300	15	4.8 ± 0.2
	10	3.1 ± 0.3

F. Directed self-assembly

Simulations of the DSA process were conducted using a theoretically informed coarse grain model previously developed to study the kinetics of assembly in the DSA hole-shrink process, which is well described elsewhere.[11,16] In brief, n BCP chains are represented by N beads connected by Gaussian springs at constant temperature and volume. There is both a bonded energy associated with the polymer chain extension as well as a nonbonded interaction which accounts for melt compressibility, interchain interactions, as well as x_{AB}, which governs the incompatibility of the two blocks. Two further terms govern the interaction of the blocks with the sidewall and bottom of the template and decay exponentially with the distance from the template. These interactions are calculated by a particle-to-mesh (PM_0) scheme where the interactions are locally tabulated within shifting cubic cells. The model is driven to equilibrium by a Monte Carlo simulation utilizing the Metropolis Criterion, where the probability of accepting a move is given by $p_{\text{acc}} = \exp(-\Delta H/(k_b T))$. Two moves are considered: single bead displacement and chain reptation.

DSA experiments were conducted by spin coating PMMA-cylinder-forming PS-*b*-PMMA (50k-*b*-20k) with $L_0 = 38$ nm on top of the iCVD hole-shrink templates. Substrates were then annealed in a nitrogen glovebox at 270 °C for 1 h before imaging on a Zeiss Merlin SEM, using the same conditions as previously described.

III. RESULTS AND DISCUSSION

A. iCVD on hole-shrink template is ultraconformal and uniform

AFM data were collected to measure the conformality of the iCVD film, as shown in Fig. 2. As the profile was flat across the bottom of the holes, a true depth could be measured. If the depth of the hole decreased, then additional material must have been deposited on the template bottom

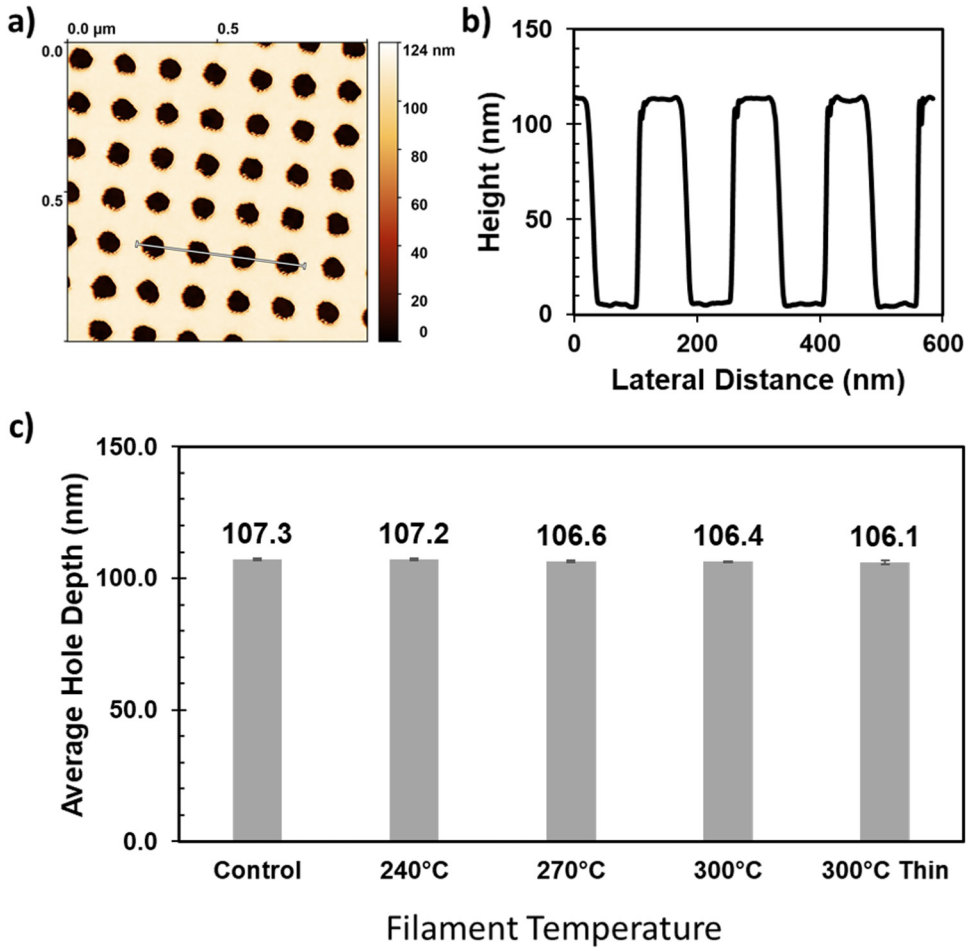

FIG. 2. (a) Representative AFM image from a hole-shrink template and (b) the extracted profile. (c) The collected hole depths as measured for a minimum of 35 holes for each thick film deposition and for the 300 °C thin film condition. Error bars represent standard deviation of 35 measurements and are less than half a nanometer in all cases.

relative to the SOC sidewalls/top. Similarly, if the depth of the hole increased, then less film must have been deposited on the template bottom relative to the SOC sidewalls/top. The thicker film depositions were measured as they were most likely to show the effect of nonconformal deposition, although a single thin condition was collected as additional validation. In all cases across more than 35 holes, the depth of the hole remained mostly constant. Some small decrease in the hole depth was measured at higher temperatures, suggesting a slightly increased film thickness on the template bottom relative to the sidewalls. The standard deviation of hole depths was also very small (<0.8 nm), indicating the uniformity of the template hole depth was also unchanged as a result of the iCVD deposition.

B. Hole-island qualitatively determines interfacial energy

Lamellae-forming BCP naturally form parallel domains when the surface energies of the blocks are unequal. Because the PS-*b*-PMMA (22k-*b*-22k) is annealed at 170 °C, PS has a lower surface energy and is pinned to the free interface.[29,30] If the interfacial energy of the substrate is lower toward PS than PMMA, PS is similarly pinned to the substrate, in a case called symmetric wetting. In symmetric wetting, the film can only form smooth parallel lamella when the film thickness is an integer multiple of L_0 (nL_0). At incommensurate spacings, the film will break to form a terraced structure. Alternatively, if the interfacial energy is close to nonpreferential, perpendicular assembly can be obtained at the interface.[26] If instead the interfacial energy of the substrate is lower toward PMMA than PS, PMMA is pinned to the substrate in a case called asymmetric wetting. In asymmetric wetting, the commensurate film thickness is offset by exactly $0.5L_0$ from the symmetric wetting case ($nL_0 + 0.5L_0$). Thus, by spin coating at thicknesses that span from the symmetric wetting commensurability condition (L_0) to the asymmetric wetting commensurability condition ($1.5L_0$), the substrate interfacial energy can be qualitatively determined. Since the substrate's preferentiality is determined relative to the free interface (symmetric versus asymmetric), it is important that this test is performed at 170 °C where the surface free energy of PS is much lower than PMMA, ensuring it prefers the free interface.

Figures 3 and 4 show the results of the hole-island test for all iCVD conditions as conducted on the SiOx and SOC

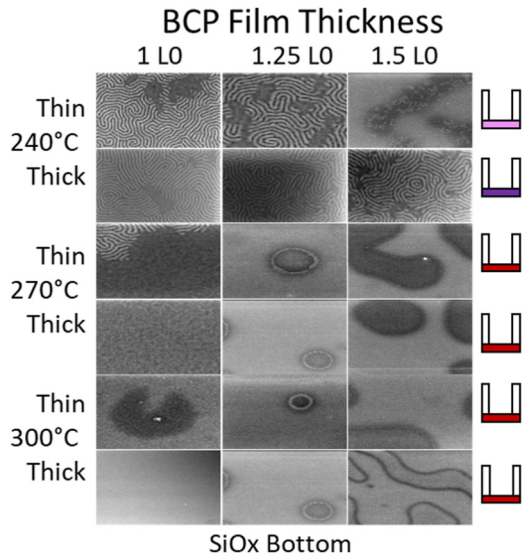

FIG. 3. SEM micrographs capturing the PS-*b*-PMMA film assembly at different thicknesses and iCVD filament temperatures and relative thicknesses (left labels) on samples of the SiOx bottom. The sketch to the right of each row of SEM images shows the strength of the sidewall preferentiality from light to dark. Red or blue (color online) indicates PS or PMMA preference, respectively.

samples, which mimic the template bottom and sidewall, respectively. A schematic depiction of preferentially is shown following the previously described rules where darker indicates stronger preferentiality indicated by the appearance of fingerprint at fewer film thicknesses. Red or blue (color online) indicates PS or PMMA preference, respectively.

Considering first only the SiOx results (Fig. 3), increasing temperature increases the PS preference in agreement with previous iCVD experiments.[19] Similarly, increasing thickness increases the PS preference. However, we see that the SOC sidewall is almost always more PMMA-preferential than the SiOx bottom (Fig. 4). Even more dramatic is that at a filament temperature of 300 °C, which was previously found to create very PS-preferential films, instead a PMMA-preferential sidewall is found for the thinner iCVD film. This can be explained only by the polymer interacting with both the iCVD film and the substrate during annealing. Previous work has shown that films in the thickness regime studied here often present interfacial energies as mixtures of both the film and substrate as the polymer can penetrate the film during annealing and interact with the substrate.[31,32] It was also recently noted that PDVB iCVD films at these thicknesses serve as ineffective barriers to resist processing, which further suggests the polymer may be able to contact the underlying substrate.[21] Several iCVD depositions appear to present interfacial energies that may be ideal for the DSA hole-shrink process. In particular, the 240 °C thin film deposition created a nonpreferential bottom with a truly PS-preferential sidewall. To better understand the true interfacial energy, quantitative measurements must be taken.

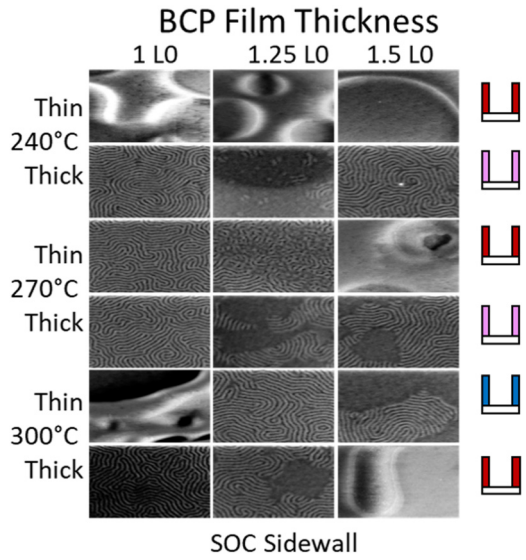

FIG. 4. SEM micrographs capturing the PS-*b*-PMMA film assembly at different thicknesses and iCVD filament temperatures and relative thicknesses (left labels) on witness samples of the SOC sidewall. The sketch to the right of each row of SEM images shows the strength of the sidewall preferentiality from light to dark.

C. Quantitative measurements confirm qualitative results

Figure 5 illustrates the effective surface energy presented by both the sidewall and bottom of the templates.

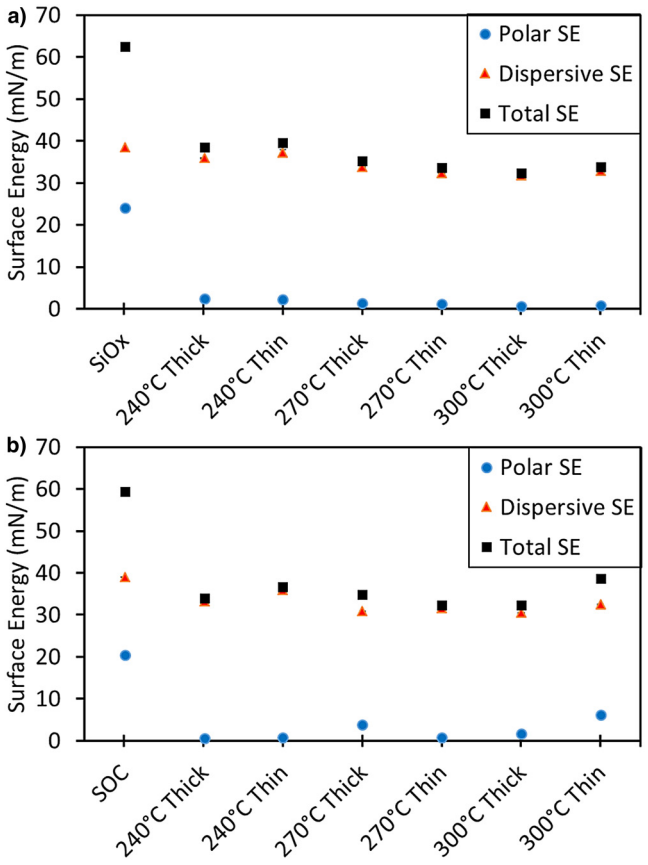

FIG. 5. Calculated polar, dispersive, and total surface energy for all iCVD conditions. (a) Silicon witness samples, which mimic the template bottom. (b) SOC witness samples, which mimic the template sidewall. Error bars represent standard deviations of three measurements and are too small to observe.

The predominant measured effect of the iCVD film is to immediately drop the polar component of surface energy. One notable outlier of this rule is the 300 °C thin deposition on SOC, which still has a large polar component. There is also a subtle difference between the surface energy of the SOC and the SiOx. To directly map the quantitative results on to the qualitative hole-island tests, the surface energy must be mapped onto an interfacial energy using the harmonic mean equation. Once the interfacial energy between the film and PS as well as the film and PMMA is calculated, the difference of these interfacial energies is calculated to quantify the substrate preferentiality.

Figure 6 shows the difference in interfacial energy along with the summarized qualitative results of the hole-island test. In the simplest case of calculating interfacial energy, we see that only the pure PS-preferential conditions are adequately captured by the quantitative calculations. To correct for the observed effect of substrate/film mixed interfacial energy, the simplest approach is to average the effect of both the substrate and the film. When this is done, the qualitative results are captured for all the other films. This definitively shows the polymer must see a mixed chemistry for many of the conditions explored here. The 240 °C thinner iCVD film, which previously appeared to be promising for DSA, is found to have the largest PS-preferential sidewall, which recently has been shown to be critical for DSA hole-shrink process latitude.[16]

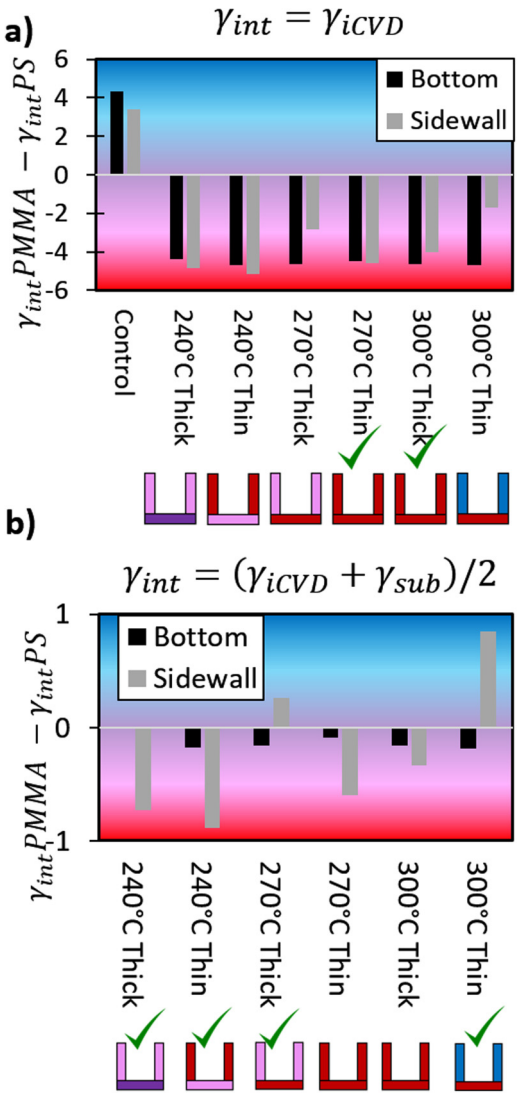

FIG. 6. (a) Calculated interfacial energies of both bottom (SiOx) and sidewall (SOC) of the template for both PS and PMMA. For clarity, only the difference in interfacial energy is plotted, with the background gradient indicating the relative strength of the preferentiality. Red or blue (color online) indicates PS or PMMA preference, respectively. (b) The same calculation under the assumption that the polymer interacts with a mixture of the film and substrate. Sketches of template chemistry as determined by the qualitative hole-island test are shown for the ease of comparison. A green check mark indicates the agreement between quantitative and qualitative results.

D. Simulation and experiment agree that the 240 °C thin iCVD film is ideal for DSA hole-shrink

As a final test, DSA was simulated and performed in experiments on the ideal 240 °C iCVD thin film sample identified in the qualitative and quantitative tests (Fig. 7). The simulation showed no defective structures, e.g., bridging across a large range of template sizes. At larger sizes, donuts eventually formed, which began to exhibit breaks as the size continued to increase. A similar trend was observed in the case of experiments in which perfect DSA was observed up until a template diameter of 70 nm corresponding to a

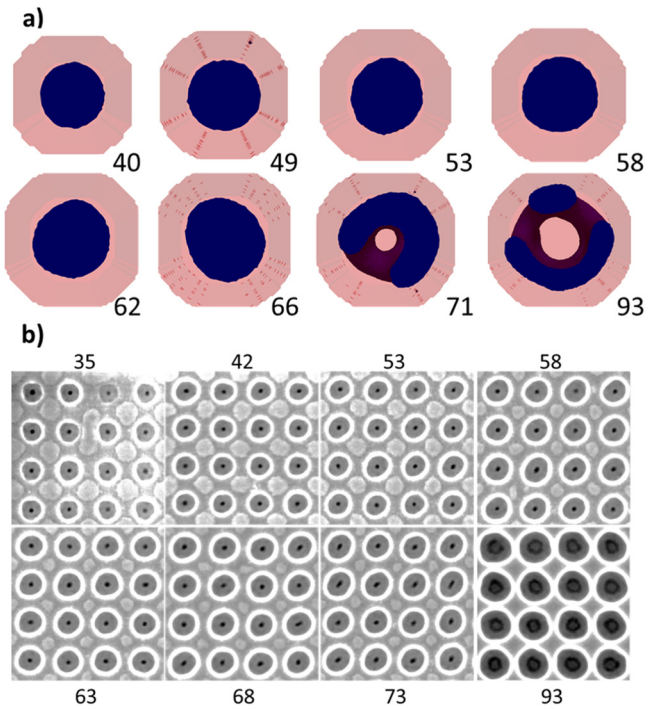

FIG. 7. Comparison of simulations and experimental results of the DSA hole-shrink process with different widths of guiding holes given in nanometers. (a) Results of simulations. (b) SEM micrographs of experimental DSA results. Both ideal assembly and the eventual formation of donut structures are captured in both experiments and simulations of the hole-shrink process on the 240 °C thin film processed template earlier identified as ideal. Note the experimental diameters have been corrected to account for the iCVD thickness. The template holes are on a 150 nm pitch that serves as an internal scale.

confinement size of 63 nm. Past this diameter, some shift was observed in the cylinder center, before finally a donut was formed at 100 nm.

Of note is the suppression of the donut morphology in experiments relative to simulation. This could be due to the partially excluded area of the iCVD film, which the BCP can sample in experiments. In comparison, the simulation considers the walls of the template to be hard walls. Another factor is the ellipticity of the template holes formed during the e-beam process due to the biaxial beam blanker. Previously, work by Iwama *et al.* used self-consistent field theory to show how ellipticity in the case of rectangular, rounded rectangular, or elliptical confinement acts to suppress the formation of defects in the DSA hole-shrink process.[33] This is because ellipticity imposes an entropic penalty on the formation of radially symmetric phases. This was further probed by Doise *et al.* using both theoretically informed coarse grained simulation and experiment, where they found that homopolymer addition was necessary to overcome this entropic penalty in order to form cylinder doublets in highly elliptical holes.[13] As simulation shows our dominant defect in this case should be the radially symmetric donut, the presence of ellipticity likely penalizes this defect mode enough to prevent its occurrence at the dimensions probed experimentally.

IV. SUMMARY AND CONCLUSIONS

In this work, we have demonstrated the ability of iCVD to be used as an all-vapor chemical functionalization strategy for the DSA hole-shrink process. Both qualitative observations and quantitative measurements revealed that at a moderate temperature, 240 °C, a strong preferential template sidewall can be created while maintaining a nonpreferential template bottom. The interfacial energies generated could be explained by considering a blending of the film interfacial energy with that of the underlying substrate. Both simulation and experiment then showed how this ideally functionalized template can easily guide DSA of cylinder-forming PS-*b*-PMMA, creating much smaller contact holes. This work opens the ability of a dry process to replace one or more complex wet processing steps without impacting the DSA process.

ACKNOWLEDGMENTS

The authors acknowledge support from the National Science Foundation (Award No. 1344891). Use of the Institute of Soldier Nanotechnologies is supported by the US Army Research Laboratory and the US Army Research Office under Contract No. W911NF-13-D-0001. This work made use of the Pritzker Nanofabrication Facility of the Institute for Molecular Engineering at the University of Chicago, which receives support from the Soft and Hybrid Nanotechnology Experimental (SHyNE) Resource (No. NSF ECCS-1542205), a node of the National Science Foundation's National Nanotechnology Coordinated Infrastructure. The authors also acknowledge the MRSEC Shared User Facilities at the University of Chicago (No. NSF DMR-1420709). They thank Gordon S. W. Craig for helpful edits.

[1]C.-C. Liu, C. J. Thode, P. A. R. Delgadillo, G. S. W. Craig, P. F. Nealey, and R. Gronheid, J. Vac. Sci. Technol. B **6**, 29 (2011).
[2]M. Somervell *et al.*, Proc. SPIE **8325**, 1 (2012).
[3]M. H. Somervell *et al.*, Proc. SPIE **8682**, 1 (2013)
[4]Y. Seino *et al.*, J. Micro/Nanolithogr. MEMS MOEMS **12**, 033011 (2013).
[5]H. Yi, X. Y. Bao, R. Tiberio, and H. P. Wong, Nano Lett. **15**, 805 (2015).
[6]C.-C. Liu *et al.*, Nat. Electron. **10**, 1 (2018).
[7]C. Chi *et al.*, Proc. SPIE **10146**, 101460Q (2017).
[8]J. Doise, J. Bekaert, B. T. Chan, M. Hori, and R. Gronheid, J. Micro/Nanolithogr. MEMS MOEMS **16**, 023506 (2017).
[9]R. Gronheid, M. Hori, B. T. Chan, and J. Doise, J. Micro/Nanolithogr. MEMS MOEMS **3**, 16 (2017).
[10]R. Gronheid, C. Boeckx, J. Doise, J. Bekaert, I. Karageorgos, J. Ruckaert, B. T. Chan, C. Lin, and Y. Zou, Proc. SPIE **9776**, 97761W (2017).
[11]C. Zhou *et al.*, J. Micro/Nanolithogr. MEMS MOEMS **17**, 031203 (2018).
[12]C. K. Hohle *et al.*, Proc. SPIE **10146**, 1 (2017).
[13]J. Doise, C. Bezik, M. Hori, J. J. de Pablo, and R. Gronheid, ACS Nano **4**, 13 (2019).
[14]B. Yu, P. Sun, T. Chen, Q. Jin, D. Ding, B. Li, and A. C. Shi, Phys. Rev. Lett. **13**, 96 (2006).
[15]N. Laachi, K. T. Delaney, B. Kim, S.-M. Hur, R. Bristol, D. Shykind, C. J. Weinheimer, and G. H. Fredrickson, J. Polym. Sci. B Polym. Phys. **2**, 53 (2015).
[16]C. T. Bezik, G. P. Garner, and J. J. de Pablo, Macromolecules **7**, 51 (2018).
[17]A. T. Servi, E. Guillen-Burrieza, D. M. Warsinger, W. Livernois, K. Notarangelo, J. Kharraz, J. H. Lienhard V, H. A. Arafat, and K. K. Gleason, J. Membr. Sci. **523** (2017).
[18]P. Moni, A. C. Mohr, and K. K. Gleason, Langmuir **23**, 34 (2018).
[19]P. Moni, H. S. Suh, M. Dolejsi, D. H. Kim, A. C. Mohr, P. F. Nealey, and K. K. Gleason, Langmuir **15**, 34 (2018).
[20]P. Moni, A. Al-Obeidi, and K. K. Gleason, Beilstein J. Nanotechnol. **8**, 723 (2017).
[21]H. S. Suh, D. H. Kim, P. Moni, S. Xiong, L. E. Ocola, N. J. Zaluzec, K. K. Gleason, and P. F. Nealey, Nat. Nanotechnol. **6**, 12 (2017).
[22]G. Ozaydin-Ince and K. K. Gleason, J. Vac. Sci. Technol. A **5**, 27 (2009).
[23]M. J. Maher, J. L. Self, P. Stasiak, G. Blachut, C. J. Ellison, M. W. Matsen, C. M. Bates, and C. G. Willson, ACS Nano **10**, 10152 (2016).
[24]R. D. Peters, X. M. Yang, and P. F. Nealey, Macromolecules **5**, 35 (2002).
[25]A. P. Smith, J. F. Douglas, J. C. Meredith, E. J. Amis, and A. Karim, J. Polym. Sci. Polym. Phys. **18**, 39 (2001).
[26]H. S. Suh, H. Kang, P. F. Nealey, and K. Char, Macromolecules **10**, 43 (2010).
[27]W. E. Tenhaeff and K. K. Gleason, Langmuir **12**, 23 (2007).
[28]S. Wu, *Polymer Interface and Adhesion* (Taylor and Francis, New York, 2017).
[29]P. Mansky, Science **5305**, 275 (1997).
[30]E. Han, K. O. Stuen, M. Leolukman, C.-C. Liu, P. F. Nealey, and P. Gopalan, Macromolecules **13**, 42 (2009).
[31]S. Xiong, Y. A. Chapuis, L. Wan, H. Gao, X. Li, R. Ruiz, and P. F. Nealey, Nanotechnology **41**, 27 (2016).
[32]E. Han, K. O. Stuen, Y.-H. La, P. F. Nealey, and P. Gopalan, Macromolecules **23**, 41 (2008).
[33]T. Iwama, N. Laachi, K. T. Delaney, B. Kim, S.-M. I. Hur, R. Bristol, D. Shykind, C. J. Weinheimer, and G. H. Fredrickson, J. Photopolym. Sci. Technol. **1**, 26 (2013).